Structure–Property Correlations in Hybrid Polymer–Nanoparticle Electrospun Fibers and Plasmonic Control over their Dichroic Behavior

Nikhil Sharma,[†] Steven J. McKeown,[‡] Xin Ma,[‡] Darrin J. Pochan,[†] and Sylvain G. Cloutier[‡,*]

[†]Department of Materials Science and Engineering, 201 DuPont Hall, University of Delaware, Newark, Delaware 19716 and [‡]Department of Electrical and Computer Engineering, 310 DuPont Hall, University of Delaware, Newark, Delaware 19716

ABSTRACT Electrospinning constitutes a simple and versatile approach of fabricating polymer heterostructures composed of nanofibers. A preferred alignment of polymer crystallites stems from complex shear elongational forces and generates a strong intrinsic optical anisotropy in typical electrospun fibers of semicrystalline polymers. While it can prove useful for certain devices, this intrinsic anisotropy can be extremely detrimental for other key applications such as high-performance polymer-based lighting and solar-energy harvesting platforms. We report a dramatic reduction in the intrinsic dichroism of electrospun poly(ethylene oxide) fibers resulting from the incorporation of inorganic nanoparticles in the polymer matrix. This effect is shown to originate from a controllable randomization of the orientational ordering of the crystalline domains in the hybrid nanofibers and not merely from a reduction in crystallinity. This improved understanding of the crystalline structure–optical property correlation then leads to a better control over the intrinsic anisotropy of electrospun fibers using localized surface-plasmon enhancement effects around metallic nanoparticles.

KEYWORDS: electrospinning · dichroism · nanoparticles · fibers · arrays · orientation · polymer–nanoparticle hybrids · nanocomposites · optical anisotropy · surface plasmon resonance

In recent years, electrospinning[1,2] has become a powerful fabrication method for constructing high aspect ratio polymer or inorganic nanostructures used to manufacture complex hybrid architectures with applications in areas ranging from catalysis,[3] sensing,[4] waveguiding,[5] and optoelectronics[6,7] to tissue-engineering constructs.[8] Modifications made to the conventional electrospinning geometry further extend the breadth of fabrication capability afforded by this technique.[9–14] Furthermore, the use of electrospinning for the construction of polymer films presents certain advantages over spin coating. For instance, the ability to form multilayer architectures[10] without reintroducing solvent into contact with sublayers is a unique feature of film formation *via* electrospinning. During electrospinning, a polymer solution of suitable viscosity is typically pumped through a metal capillary charged at high voltages. A strong electric field acts on the pendant polymer droplet to overcome surface tension and generate a characteristic whipping jet that loses solvent *via* rapid vaporization while traveling toward a grounded target, resulting in polymer nanofibers with uniquely high surface-to-volume ratio.[15] Typical electrospun fibers have been previously shown to possess optical anisotropy.[16,17] In conventional polymer systems, structural and optical anisotropy is generally introduced through strains,[18] heating,[19] or grafting chains on a surface.[20] The process of mechanical drawing can also induce a significant anisotropy in polymer films or fibers due to a preferred orientation of the polymer chains within the films or fibers[21–23] and often poses major impediments in traditional polymer engineering. For typical electrospun fibers of semicrystalline polymers, this intrinsic optical anisotropy[16,24] originates from the high shear forces acting on the electrified polymer jet during electrospinning that leads to an orientation of polymer crystallites within the fibers. While this intrinsic optical anisotropy can prove useful for certain devices, it can be detrimental in other key applications such as high-performance polymer-based lighting and solar-energy harvesting platforms.

In this paper, we report a dramatic reduction in the intrinsic optical anisotropy of electrospun poly(ethylene oxide) nanofibers resulting from the incorporation of different concentrations of silica nanoparticles in the polymer matrix. Interestingly, X-ray diffraction combined with differential scanning calorimetry measurements confirm that this decrease in intrinsic

*Address correspondence to cloutier@udel.edu.

Received for review November 23, 2009 and accepted August 31, 2010.

Published online September 13, 2010.
10.1021/nn100582f

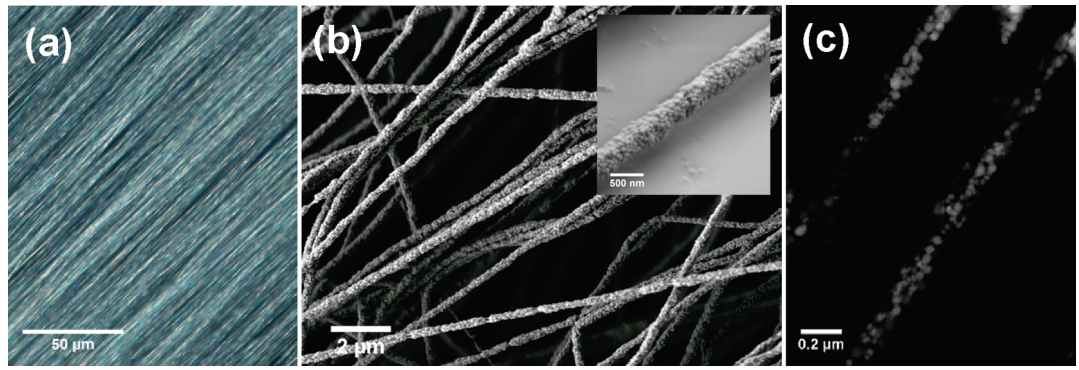

Figure 1. (a) Optical micrograph of highly oriented electrospun PEO fibers loaded with silica nanoparticles. (b) Scanning electron microscopy image of PEO fibers highly loaded with 50 nm silica particles. Inset shows a high-magnification SEM image of a fiber with encapsulated silica nanoparticles. (c) High-angle annular dark-field scanning transmission electron micrograph (HAADF-STEM) image of hybrid fibers showing arrangement within the polymer fiber.

anisotropy originates from a controllable randomization of the orientational ordering of the crystalline domains in the hybrid nanofibers and not merely from a reduction in crystallinity. Finally, the improved understanding of their crystalline structure−optical property correlation leads us to develop a better control over the intrinsic anisotropy of electrospun fibers using resonant localized surface-plasmon enhancement effects resulting from the incorporation of a minute fraction of metallic nanoparticles. While previous reports of constructing hybrid composites *via* electrospinning have demonstrated the unique capability of this versatile fabrication approach,[25−31] we believe this ability to controllably alter the intrinsic anisotropy of electrospun fibers yields crucial insight into the fundamental correlation between their structure and physical behavior. This deeper understanding facilitates better materials design and in turn the deployment of electrospun systems as thin film materials in emerging applications.

RESULTS AND DISCUSSION

First, silica nanoparticles are blended into an aqueous polyethylene oxide (PEO) solution so that electrospinning yields hybrid polymer nanofibers with confined nanoparticles inside the PEO matrix. The use of a collector electrode with an air gap alters the electric field lines causing a preferred alignment of incoming fibers perpendicular to the gap edge.[32] These highly aligned hybrid nanofibers are shown in the optical microscopy image in Figure 1a. A typical scanning electron microscopy (SEM) image of the hybrid nanofibers highly loaded with 50 nm SiO_2 nanoparticles is shown in Figure 1b. The high-magnification inset in Figure 1b shows the quasi-1D organization of the silica nanoparticles inside the fibers owing to their smaller size compared to the fiber diameter. High-angle annular dark-field scanning transmission electron microscopy (HAADF-STEM) shown in Figure 1c confirms that the silica nanoparticles are not located only on the surface of the fibers but are encapsulated throughout the fiber volume. The PEO matrix consists of lighter elements and is scarcely visible in the micrograph.

For optical characterization, samples of highly aligned PEO fibers loaded with different concentrations of 50 nm SiO_2 nanoparticles are fabricated. To do so, silica nanoparticle dispersions of increasing concentrations are blended into a fixed amount of PEO solution before electrospinning. Favorable hydrogen-bonding interactions between the hydroxyl functionality on the silica particle surface and the PEO polymer chains allows the incorporation of high nanoparticle concentrations in the precursor solutions. Electrospinning parameters such as voltage, needle gauge, polymer concentration, and needle-collector distance are kept constant so as to not affect the resulting fiber diameter. The exact particle content within the hybrid nanofibers is then measured using thermogravimetric analysis (TGA). During TGA, the composite nanofibers are heated until a complete thermal degradation of the polymer is achieved, and the final residual mass is composed solely of the remaining nanoparticles. Figure 2 shows thermograms of a series of electrospun fibers with increasing nanoparticle content. Differential scan-

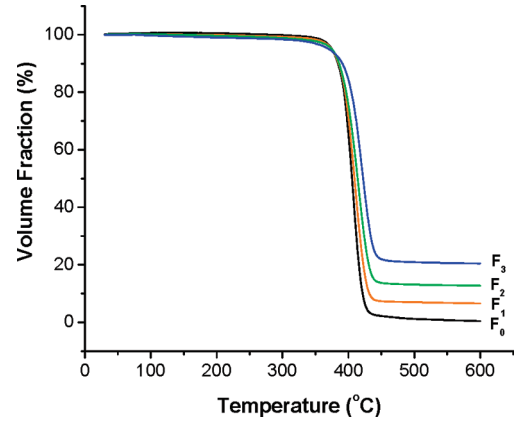

Figure 2. Thermogravimetric curves of particle-dosed fiber series. Final residual mass indicates incorporated silica nanoparticle content. Samples F_0, F_1, F_2, and F_3 are PEO fibers with 0 (neat fibers), 7, 12, and 20 vol % incorporated silica content, respectively.

TABLE 1. Fiber Construction Parameters, Incorporated Silica Nanoparticle Content Determined by TGA, Melting Enthalpies and Polymer Degree of Crystallinity Determined by DSC, and Fiber Diameters Determined by SEM

sample designation	volume of PEO soln (50 mg/mL)	concentration of SiO_2 nanoparticle dispersion (0.5 mL, 50 nm)	incorporated SiO_2 content (vol %)[a]	melting enthalpy (ΔH_m) of fiber samples (J/g)[b]	PEO degree of crystallinity (%)[b]	fiber diameter (nm)[c]
F_0	1.5 mL	0 mg/mL (DI water)	0	197	97.2 ± 0.3	216 ± 35
F_1	1.5 mL	10 mg/mL	7.0 ± 0.8	196.6	97 ± 1.5	183 ± 44
F_2	1.5 mL	25 mg/mL	12.1 ± 1	187.6	92 ± 1.9	194 ± 30
F_3	1.5 mL	50 mg/mL	20.4 ± 0.1	191.4	94 ± 0.3	190 ± 37

[a]As determined by TGA. [b]As determined by DSC. [c]As determined by SEM.

ning calorimetry (DSC) was conducted on the fiber samples to investigate the degree of crystallinity of the polymer within the composite fiber samples. Fiber construction parameters, incorporated nanoparticle content (as determined by TGA), melting enthalpies of the composite fibers, and the degree of crystallinity of the polymer fraction of the fiber samples (as determined by DSC) as well as fiber diameters (as determined by SEM) are summarized in Table 1.

The dichroic ratio for the hybrid fibers with different nanoparticle concentrations is obtained by measuring the relative absorption of the orthogonal components (parallel and perpendicular to fiber axis) of incident circularly polarized light. A schematic of the optical setup is shown in Figure 3a. Dichroic ratios were found by measuring the fibers' interaction with circularly polarized light by using a polarizer to measure components parallel and perpendicular to the fiber axis. Dichroic ratio (DR) is defined as the ratio of absorptions in parallel and perpendicular configurations using the following expression:

$$\mathrm{DR} = \frac{A_{\parallel}}{A_{\perp}} = \frac{\ln(I_0/I)_{\parallel}}{\ln(I_0/I)_{\perp}} \quad (1)$$

where A is the absorption measured for orthogonal parallel ($\parallel$) and perpendicular ($\perp$) polarizations with respect to the fibers' axis and is defined as the ratio of incident (I_0) and transmitted intensities (I) for both polarizations. Three individual DR measurements performed on the neat PEO and PEO−SiO_2 samples as well as their average are plotted in Figure 3b as a function

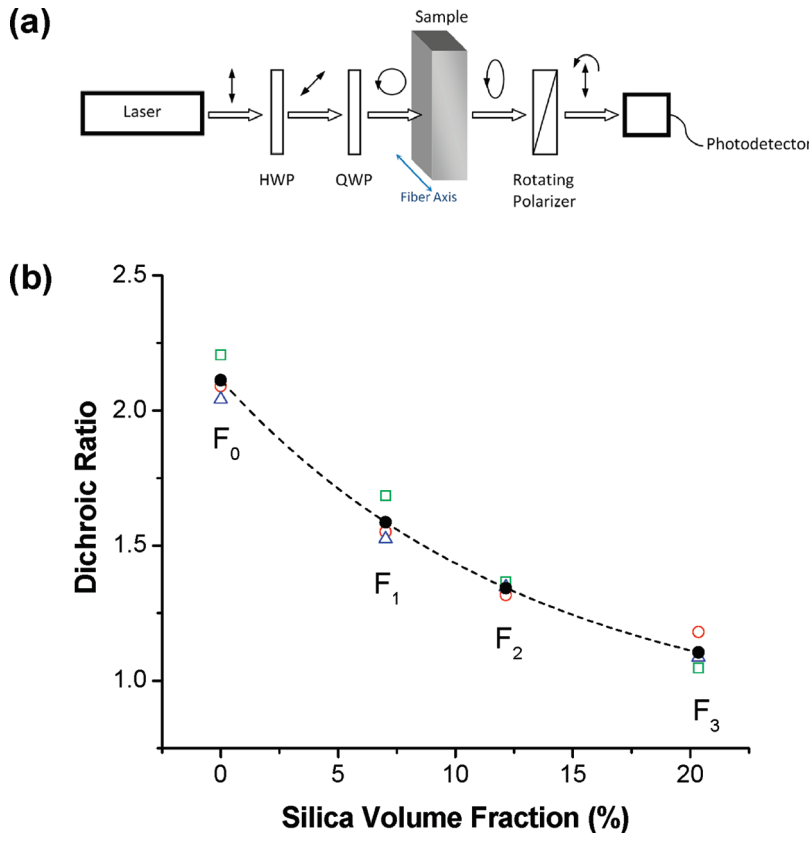

Figure 3. (a) Schematic of the optical setup used to measure dichroic ratio of the aligned electrospun fibers. (b) Chart showing the relationship between dichroic ratio [measurement 1 (□), measurement 2 (○), measurement 3 (Δ), mean (●)] of particle-loaded fiber series (λ = 633 nm) and silica volume fraction.

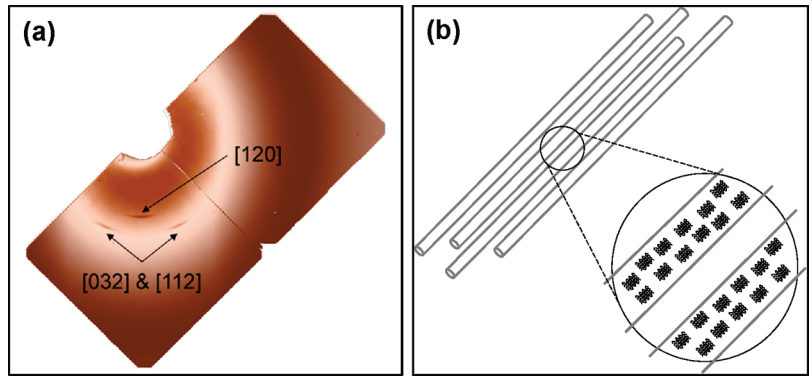

Figure 4. (a) 2D X-ray diffraction pattern of sample F_0 (neat PEO fibers). Diffraction peaks for planes [120] (at $2\theta = 10.1°$) and [032], [112] (at $2\theta = 12.3°$) are marked by arrows. (b) Schematic (not drawn to scale) showing oriented crystallite arrangement within neat PEO fibers. The white spaces between the polymer crystallites represent regions of amorphous polymer domains.

of the silica volume fraction. An exponential decay in intrinsic optical dichroism, indicated by the dotted curve in Figure 3b, can be consistently observed for the hybrid nanofibers with increasing particle concentration. This result is consistent with optical anisotropy reduction effects reported previously for other polymer films doped with nanoparticles.[33]

It is possible to elucidate the origin of the intrinsic dichroism in the electrospun fibers by X-ray diffraction (XRD) analysis of the aligned fibers. The 2D X-ray diffraction patterns for the aligned fibers F_0 (neat PEO) is shown in Figure 4a. Since PEO is a semicrystalline polymer that crystallizes most commonly in the $^7/_2$ helical conformation,[34] strong monoclinic reflections occurring at $2\theta = 10.1°$ (corresponding to plane [120]) and 12.3° (corresponding to planes [032], [112])[26,35] are observed on the meridional sector for both samples. A perfectly isotropic distribution of crystalline domains would yield powder diffraction maxima (polycrystalline ring-like diffraction pattern), with no azimuthal dependence in the intensity profile, while a preferred orientational ordering of the crystalline domains results in an anisotropic diffraction pattern. The amorphous nature of the silica nanoparticles does not yield an X-ray diffraction signature, which could otherwise convolute XRD analysis. The diffraction pattern for the F_0 sample shown in Figure 4a confirms a preferred orientation of the polymer crystalline domains along the fiber axis. A schematic of the polymer morphology inside those fibers is shown in Figure 4b where the white spaces between the polymer crystallites represent regions of amorphous polymer domains. This directional ordering of the crystallites within the fibers originates from complex elongational shear forces acting on the electrified polymer fluid jet during electrospinning[24,36] and is consistent with previous results.[35,37,38] Thus in the case of neat PEO fibers, the optical absorption for incident light polarized along the fibers' axis is greatly enhanced compared to perpendicularly polarized light.

In contrast, a clear structural change can be observed for the fibers loaded with silica nanoparticles. The X-ray diffraction pattern for sample F_3 (20 vol % SiO_2 in PEO) is shown in Figure 5a. Diffraction maxima now spread over a broader range of azimuthal angles suggesting crystal planes oriented off-axis relative to the fiber alignment axis causing a higher degree of orientational randomization. It is important to note that in both cases the fibers are macroscopically aligned along the same axis relative to the incident X-rays. Yet, a more isotropic arrangement of the crystalline domains is clearly observed in the diffraction pattern for the particle-loaded fibers. Graphs comparing the azimuthal distribution of scattered intensity for the neat and particle-loaded fibers are shown in Figure 5b, where radial intensity profiles at scattering angle, $2\theta = 10.1°$ and 12.3°, are plotted as a function of the azimuthal angle (β) for samples F_0 and F_3. The *x*-axis is scaled in pixels but corresponds to β values ranging from 0° (for pixel 0) to 90° (for highest pixel value), considering only the meridional sector of the diffractogram. For $2\theta = 10.1°$, the intensity profile for F_0 shows sharper maxima than for F_3 at $\beta \approx 45°$, and at $2\theta = 12.3°$ the profile for F_0 shows symmetric peaks corresponding to $\beta \approx 22.5°$ and 67.5°, whereas a relatively isotropic intensity profile is observed for F_3. A schematic of the polymer morphology inside particle-loaded hybrid fibers is shown in Figure 5c to illustrate how the introduction of silica nanoparticles into the fibers perturbs the orientational ordering of the polymer crystalline domains. These results confirm that the dichroic ratio of the nanoparticle-loaded fibers decays due to an increasing departure from the well-oriented state of the crystallites in the neat fibers toward a more isotropic phase. Importantly, these results suggest that the decrease in dichroic ratio is not simply a consequence of lower crystallinity originating from nanoparticle-incorporation into the polymer matrix but stems from a perturbation-induced reorganization of the polymer crystallites around the nanoparticles. DSC results shown in Table 1 also corroborate that the PEO degree of crystallinity decreases by only a marginal amount with increasing nanoparticle content. This assertion is further supported by an analysis of the dichroic behavior of fibers loaded

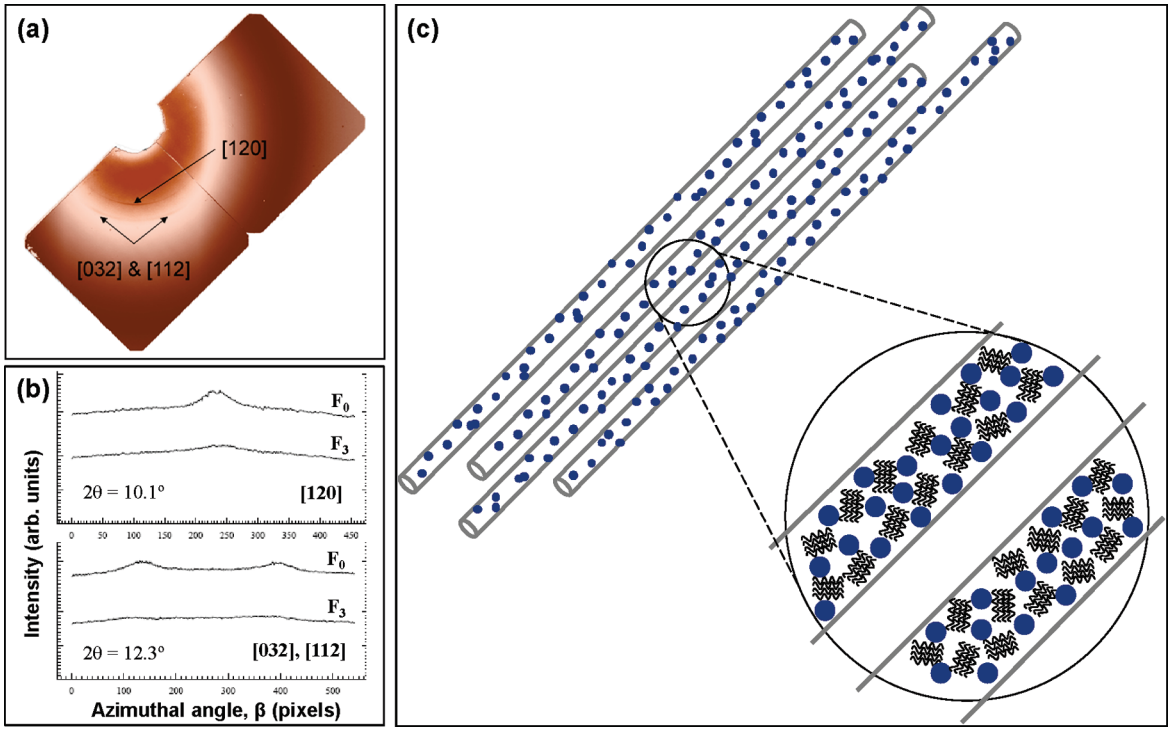

Figure 5. (a) 2D X-ray diffraction pattern of sample F_3 (PEO fibers containing 20 vol% SiO_2 nanoparticles). (b) Scattered intensity as a function of azimuthal angle, β (scaled in pixels, ranging from 0 to 90 deg of the meridional sector) for samples F_0 and F_3. Top graph shows azimuthal profile at scattering angle $2\theta = 10.1°$, and bottom graph shows azimuthal profile at $2\theta = 12.3°$. (c) Schematic (not drawn to scale) showing perturbation of crystalline-domain orientation due to the incorporated silica nanoparticles into the fiber matrix.

with very minute fractions of gold nanoparticles, as discussed next.

Now, we demonstrate a concrete example of how this clear understanding of the fundamental correlation between the crystalline structure and optical properties of hybrid electrospun fibers can lead to better ways of controlling the optical anisotropy of electrospun fibers. Indeed, the incorporation of minute quantities of metallic nanoparticles into the same PEO electrospun fiber matrix can cause an even greater reduction in the overall dichroic ratio than with 2 orders of magnitude larger concentrations of silica nanoparticles. While the gold nanoparticles cause a local perturbation of the crystalline domains similar to the silica case described above, the consequences of this particle-induced disordering of the polymer crystallites are strongly enhanced by the electromagnetic field-enhancement due to localized surface-plasmon oscillations around the metallic nanostructures. This result confirms that the decrease in dichroic ratio indeed occurs from a perturbation in domain-orientation as the amount of gold nanoparticles incorporated into the fiber matrix is minuscule which thus has a negligible effect on overall crystallinity of the polymer fibers, in comparison to neat fibers. However, since the areas of domain-reorientation lie in regions of a plasmonically enhanced field this results in an effective decrease in dichroic ratio without a decrease in overall crystallinity or a substantial loss of polymer mass.

To fabricate the gold nanoparticle-loaded PEO fibers, 50 nm citrate-capped gold nanoparticles are introduced in the polymer precursor prior to electrospinning. The electrospinning of the gold-loaded hybrid fibers (designated F_A) was performed under identical conditions as for the silica-loaded samples. TGA analysis on this sample yields a nanoparticle incorporation of ~0.2 vol %, as shown in Figure 6a. The low gold nanoparticle loading measured by TGA is consistent with the HAADF-STEM micrograph displayed in the inset in Figure 6a where gold nanoparticles appear with high contrast compared with the polymer owing to a much higher atomic number. DSC analysis yields a melting enthalpy of 192 J/g, which is very close to that of neat PEO (197 J/g), and the obtained degree of crystallinity for the gold loaded fibers is 94%.

The presence of the gold nanoparticles produces a strong plasmonic enhancement of the optical absorption of the PEO matrix as shown in Figure 6b, where the absorption curves of neat PEO and gold-loaded PEO in the visible regime are compared. The absorption band for sample F_A is centered at 545 nm and corresponds to the surface plasmon resonance peak for 50 nm gold particles surrounded by PEO. The reduction in the dichroic ratio for the sample F_A (gold) and F_3 (silica) are measured at three wavelengths (456, 532, and 633 nm) as indicated by arrows in Figure 6b. The degree of reduction in dichroism (DOR) introduced in Figure 6c can be defined as the normalized deviation from the intrin-

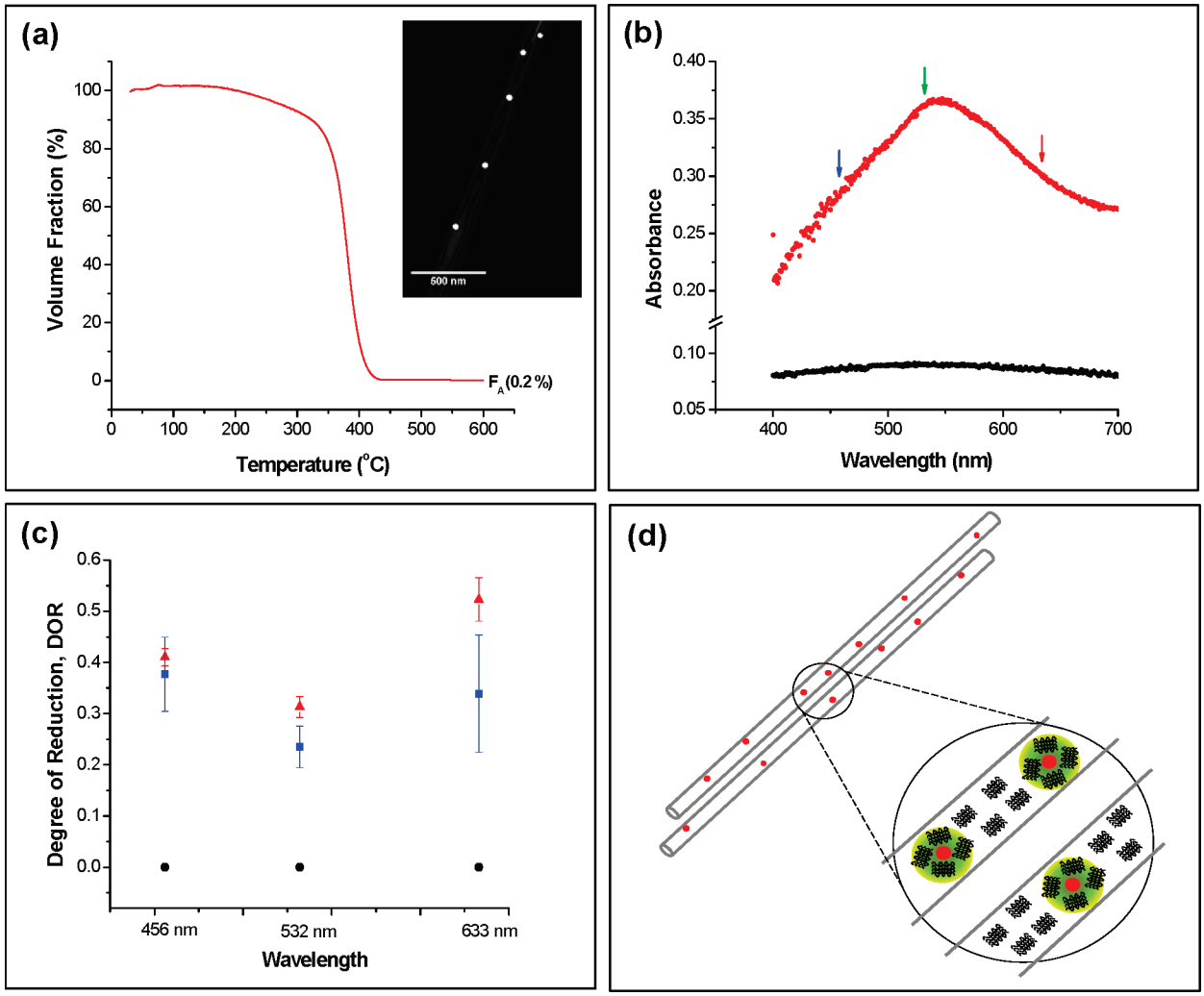

Figure 6. (a) Chart showing thermogravimetric curve for gold-nanoparticle loaded fibers (F_A). Inset shows HAADF-STEM image showing electrospun PEO fiber with encapsulated gold nanoparticles. (b) Visible absorption spectrum of neat PEO fibers (F_0, black curve) and gold-loaded PEO fibers (F_A, red curve). Arrows indicate wavelengths at which degree of reduction was measured. (c) Chart showing degree of reduction (DOR) for samples F_0 (●), F_3 (■), and F_A (▲). (d) Schematic (not drawn to scale) showing gold nanoparticles encapsulated inside macroscopically aligned PEO fibers, magnified view shows the plasmonically labeled regions of disorder. Regions of enhanced field localized around nanoparticles are indicated by green clouds.

sic dichroic ratio of neat PEO fibers and is given by the following expression:

$$\mathrm{DOR} = \frac{\mathrm{DR}_{F0} - \mathrm{DR}_F}{\mathrm{DR}_{F0}} \qquad (2)$$

where DR_F is the dichroic ratio for particle-loaded samples F_A (gold) or F_3 (silica) and DR_{F0} is the intrinsic dichroic ratio for neat PEO fibers. For nanoparticles of similar size (50 nm), the DOR measurements shown in Figure 6c confirm that minute fractions of gold (0.2 vol %) incorporated in the electrospun fibers cause a loss in dichroism comparable to what is achieved using 20 vol % of silica nanoparticle loading. Figure 6d shows a schematic illustrating the mechanism underlying the dramatic reduction in dichroism observed for electrospun fibers loaded with low fractions of gold nanoparticles. The gold nanoparticles cause a local perturbation of the crystalline domains in a manner similar to the silica-loaded fibers. However, the effect of the disordering of the polymer crystallites in the immediate vicinity of the gold nanoparticles on the optical properties of the nanocomposite is strongly enhanced by the electromagnetic field-localization due to surface-plasmon modes around the metallic nanostructures, causing a dramatic decrease in their dichroic ratio. Therefore, this metal−nanoparticle incorporation scheme can provide a powerful method for controlling the dichroic behavior of the electrospun fibers since it efficiently reduces the intrinsic optical anisotropy of electrospun polymer fibers without losing the critical polymer mass associated with the incorporation of large volume fractions of silica nanoparticles.

CONCLUSIONS

Electrospinning represents a robust nanofabrication technique of producing high-quality polymer thin films. However, a preferred orientation of polymer crystal-

lites due to shear elongational forces during electrospinning generates a strong intrinsic optical anisotropy in typical electrospun fibers, which can be problematic for certain key thin film applications. We have demonstrated an effective method for the reduction in optical anisotropy of electrospun fibers *via* the incorporation of nanoparticles. Using silica nanoparticles, we have shown that the intrinsic dichroic ratio of the hybrid polymer−particle fibers can be controllably reduced by changing the nanoparticle concentration within the fibers. We have used X-ray diffraction and differential scanning calorimetry to confirm that this atypical behavior originates from changes in the crystalline domain-orientation around the nanoparticles, and not merely from a marginal reduction in their overall crystallinity. The understanding of this crucial correlation between the structural morphology of polymer−nanoparticle hybrid fibers and their optical properties enabled the development of a unique plasmonic control strategy over the dichroic behavior of the electrospun fibers. The incorporation of minute amounts of gold nanoparticles (0.2 vol %) causes the dramatic reduction of intrinsic dichroism without losing critical polymer mass, comparable to the reduction observed with 20 vol % silica nanoparticles. This occurs because gold nanoparticles plasmonically label regions of crystalline disorder by preferentially localizing the incident field at disordered sites and cause a dramatic decrease in the dichroic ratio. We believe this unique material−design strategy will help facilitate the integration of electrospun films in polymer-based optoelectronic platforms.

METHODS

Construction of Hybrid Fiber Arrays. SiO_2 nanoparticle dispersions (0.5 mL) of increasing concentrations (0, 1, 2.5, 5 w/v %) were added to 1.5 mL of an aqueous poly(ethylene oxide) (M.W. 900 000 g/mol) solution and stirred to allow homogenization. The SiO_2 nanoparticles bear silanol functional groups on their surface. A split collector electrode was constructed by placing plastic spacers between two rectangular aluminum bars that were then taped together to form an air gap of 1.2 cm. A syringe pump was utilized for pumping the precursor solution through a 21 gauge metal needle (inner diameter, 0.51 mm), and flow rate was optimized to give a stable electrospinning jet. Electrospinning voltage was set at +12 kV by biasing the metal needle and setting the split collector electrode as ground. Fibers with encapsulated gold particles were constructed in an identical manner by blending a gold nanoparticle dispersion (0.5 mL, 0.2 μg/mL) with 1.5 mL of an aqueous PEO solution. Gold nanoparticles were stabilized by sodium citrate attached to their surface.

Characterization of Hybrid Fiber Arrays. Optical microscopy was conducted on the fibers using a Zeiss Axioskop 2 microscope. Fibers were imaged by the JEOL JSM-7400F SEM operating at voltages in the range 1−3 kV, in the standard (LEI) and secondary (SEI) mode at working distances of 3−8 mm. The fiber encapsulated nanoparticle assemblies were stuck to aluminum stubs using adhesive carbon tape and sputtered with a thin layer of Au prior to imaging. Thermogravimetric analysis was performed on the nanoparticle-dosed fibers using the Perkin-Elmer Pyris 1 TGA. Dry nitrogen was used as the purge gas, and thermograms were generated by heating the sample from room temperature to 600 °C at the rate of 10 °C/min. The sample was then held at 600 °C for 2 min. Differential scanning calorimetry was conducted on a Perkin-Elmer Diamond DSC. Helium was used as purge gas, and samples were heated to 100 °C at the rate of 10 °C/min and held at 100 °C for 2 min. An indium reference sample was utilized for calibrating the DSC. Degree of crystallinity of the samples was calculated by comparing the melting enthalpy of the sample (area under the melting peak in the DSC thermogram normalized per unit mass of polymer in the sample, as determined by TGA) with the melting enthalpy of a PEO sample with 100% crystallinity, 203 J/g.[39] X-ray diffraction data were collected at the DND-CAT Synchrotron Research Center, Advanced Photon Source at the Argonne National Laboratory. Wavelength of X-rays from the synchrotron source was 0.82656 Å. Color enhancement of the diffractograms was performed using a gradient overlay over the raw data to improve image contrast using Photoshop software. Azimuthal plots were obtained using FIT2D software by taking arc slices whose arc-coordinates (scattering angle) were kept constant across diffractograms.

Acknowledgment. We acknowledge funding support from the Army Research Laboratory CMR-CCMT332157 (Pochan) and the DARPA-Young Faculty Award program (Cloutier). We are thankful to Dr. Kirk Czymmek (Delaware Biotechnology Institute Bioimaging Center) and the W. M. Keck Foundation for its support of the Electron Microscopy Lab at the University of Delaware. We thank Dr. Chaoying Ni for assistance with electron microscopy. A portion of this work was performed at the DuPont-Northwestern-Dow Collaborative Access Team (DND-CAT) located at Sector 5 of the Advanced Photon Source (APS). DND-CAT is supported by E. I. DuPont de Nemours & Co., The Dow Chemical Company, and the State of Illinois. Use of the APS was supported by the U.S. Department of Energy, Office of Science, Office of Basic Energy Sciences, under Contract No. DE-AC02-06CH11357. We acknowledge the support of Dr. Steven Weigand for X-ray data acquisition.

REFERENCES AND NOTES

1. Reneker, D. H.; Chun, I. Nanometre Diameter Fibres of Polymer Produced by Electrospinning. *Nanotechnology* **1996**, *7*, 216–223.
2. Li, D.; Xia, Y. N. Electrospinning of Nanofibers: Reinventing the Wheel. *Adv. Mater.* **2004**, *16*, 1151–1170.
3. Li, D.; Xia, Y. Fabrication of Titania Nanofibers by Electrospinning. *Nano Lett.* **2003**, *3*, 555–560.
4. Liu, H.; Kameoka, J.; Czaplewski, D. A.; Craighead, H. G. Polymeric Nanowire Chemical Sensor. *Nano Lett.* **2004**, *4*, 671–675.
5. Liu, H. Q.; Edel, J. B.; Bellan, L. M.; Craighead, H. G. Electrospun Polymer Nanofibers as Subwavelength Optical Waveguides Incorporating Quantum Dots. *Small* **2006**, *2*, 495–499.
6. Di Benedetto, F.; Camposeo, A.; Pagliara, S.; Mele, E.; Persano, L.; Stabile, R.; Cingolani, R.; Pisignano, D. Patterning of Light-Emitting Conjugated Polymer Nanofibers. *Nat. Nanotechnol.* **2008**, *3*, 614–619.
7. Moran-Mirabal, J. M.; Slinker, J. D.; DeFranco, J. A.; Verbridge, S. S.; Ilic, R.; Flores-Torres, S.; Abrua, H. c.; Malliaras, G. G.; Craighead, H. G. Electrospun Light-Emitting Nanofibers. *Nano Lett.* **2007**, *7*, 458–463.
8. Xie, J.; MacEwan, M. R.; Li, X.; Sakiyama-Elbert, S. E.; Xia, Y. Neurite Outgrowth on Nanofiber Scaffolds with Different Orders, Structures, and Surface Properties. *ACS Nano* **2009**, *3*, 1151–1159.
9. Li, D.; Xia, Y. N. Direct Fabrication of Composite and Ceramic Hollow Nanofibers by Electrospinning. *Nano Lett.* **2004**, *4*, 933–938.
10. Li, D.; Wang, Y. L.; Xia, Y. N. Electrospinning Nanofibers as Uniaxially Aligned Arrays and Layer-by-Layer Stacked Films. *Adv. Mater.* **2004**, *16*, 361–366.

11. McCann, J. T.; Marquez, M.; Xia, Y. Melt Coaxial Electrospinning: A Versatile Method for the Encapsulation of Solid Materials and Fabrication of Phase Change Nanofibers. *Nano Lett.* **2006**, *6*, 2868–2872.
12. Li, D.; Ouyang, G.; McCann, J. T.; Xia, Y. N. Collecting Electrospun Nanofibers with Patterned Electrodes. *Nano Lett.* **2005**, *5*, 913–916.
13. Liu, Z.; Sun, D. D.; Guo, P.; Leckie, J. O. An Efficient Bicomponent TiO_2/SnO_2 Nanofiber Photocatalyst Fabricated by Electrospinning with a Side-by-Side Dual Spinneret Method. *Nano Lett.* **2006**, *7*, 1081–1085.
14. Sharma, N.; Jaffari, G. H.; Shah, S. I.; Pochan, D. J. Orientation-Dependent Magnetic Behavior in Aligned Nanoparticle Arrays Constructed by Coaxial Electrospinning. *Nanotechnology* **2010**, *21*, 085707.
15. Shin, Y. M.; Hohman, M. M.; Brenner, M. P.; Rutledge, G. C. Electrospinning: A Whipping Fluid Jet Generates Submicron Polymer Fibers. *Appl. Phys. Lett.* **2001**, *78*, 1149–1151.
16. Fong, H.; Renekar, D. H. Elastomeric Nanofibers of Styrene−Butadiene−Styrene Triblock Copolymer. *J. Polym. Sci., Part B* **1999**, *37*, 3488–3493.
17. Catalani, L. H.; Collins, G.; Jaffe, M. Evidence for Molecular Orientation and Residual Charge in the Electrospinning of Poly(butylene terephthalate) Nanofibers. *Macromolecules* **2007**, *40*, 1693–1697.
18. Carr, P. L.; Jakeways, R.; Klein, J. L.; Ward, I. M. Tensile Drawing, Morphology, and Mechanical Properties of Poly(butylene terephthalate). *J. Polym. Sci., Part B* **1997**, *35*, 2465–2481.
19. Guadagno, L.; Naddeo, C.; Vittoria, V.; Meille, S. V. Temperature and Orientation Induced Polymorphic Behavior of Syndiotactic Polypropylene. *Macromolecules* **2005**, *38*, 8755–8764.
20. Lodge, T. P.; Fredrickson, G. H. Optical Anisotropy of Tethered Chains. *Macromolecules* **1992**, *25*, 5643–5650.
21. Fouda, I. M.; Shabana, H. M. Optical and Structural Changes in Perlon Fibers due to Different Stresses. *Eur. Polym. J.* **2000**, *36*, 823–829.
22. Choi, D. M.; White, J. L. Crystallization and Orientation Development in Fiber and Film Processing of Polypropylenes of Varying Stereoregular Form and Tacticity. *Polym. Eng. Sci.* **2004**, *44*, 210–222.
23. Tanaka, M.; Young, R. J. Molecular Orientation Distributions in Uniaxially Oriented Poly(L-lactic acid) Films Determined by Polarized Raman Spectroscopy. *Macromolecules* **2006**, *39*, 3312–3321.
24. Perkins, T. T.; Smith, D. E.; Chu, S. Single Polymer Dynamics in an Elongational Flow. *Science* **1997**, *276*, 2016–2021.
25. Wang, M.; Singh, H.; Hatton, T. A.; Rutledge, G. C. Field-Responsive Superparamagnetic Composite Nanofibers by Electrospinning. *Polymer* **2004**, *45*, 5505–5514.
26. Salalha, W.; Dror, Y.; Khalfin, R. L.; Cohen, Y.; Yarin, A. L.; Zussman, E. Single-Walled Carbon Nanotubes Embedded in Oriented Polymeric Nanofibers by Electrospinning. *Langmuir* **2004**, *20*, 9852–9855.
27. Hou, H. Q.; Reneker, D. H. Carbon Nanotubes on Carbon Nanofibers: A Novel Structure Based on Elelectrospun Polymer Nanofibers. *Adv. Mater.* **2004**, *16*, 69–73.
28. Behler, K. D.; Stravato, A.; Mochalin, V.; Korneva, G.; Yushin, G.; Gogotsi, Y. Nanodiamond-Polymer Composite Fibers and Coatings. *ACS Nano* **2009**, *3*, 363–369.
29. Pabba, S.; Sidorov, A. N.; Berry, S. M.; Yazdanpanah, M. M.; Keynton, R. S.; Sumanasekera, G. U.; Cohn, R. W. Oriented Nanomaterial Air Bridges Formed from Suspended Polymer−Composite Nanofibers. *ACS Nano* **2007**, *1*, 57–62.
30. Wang, B. B.; Li, B.; Xiong, J.; Li, C. Y. Hierarchically Ordered Polymer Nanofibers *via* Electrospinning and Controlled Polymer Crystallization. *Macromolecules* **2008**, *41*, 9516–9521.
31. Ko, F.; Gogotsi, Y.; Ali, A.; Naguib, N.; Ye, H.; Yang, G. L.; Li, C.; Willis, P. Electrospinning of Continuous Carbon Nanotube-Filled Nanofiber Yarns. *Adv. Mater.* **2003**, *15*, 1161–1165.
32. Li, D.; Wang, Y.; Xia, Y. Electrospinning of Polymeric and Ceramic Nanofibers as Uniaxially Aligned Arrays. *Nano Lett.* **2003**, *3*, 1167–1171.
33. Ohkita, H.; Abe, Y.; Kojima, H.; Tagaya, A.; Koike, Y. Birefringence Reduction Method for Optical Polymers by the Orientation-Inhibition Effect of Silica Particles. *Appl. Phys. Lett.* **2004**, *84*, 3534–3536.
34. Takahashi, Y.; Tadokoro, H. Structural Studies of Polyethers, $(-(CH_2)_m-O-)_n$. X. Crystal Structure of Poly(ethylene oxide). *Macromolecules* **1973**, *6*, 672–675.
35. Dror, Y.; Salalha, W.; Khalfin, R. L.; Cohen, Y.; Yarin, A. L.; Zussman, E. Carbon Nanotubes Embedded in Oriented Polymer Nanofibers by Electrospinning. *Langmuir* **2003**, *19*, 7012–7020.
36. Bellan, L. M.; Cross, J. D.; Strychalski, E. A.; Moran-Mirabal, J.; Craighead, H. G. Molecular Orientation in Individual Electrospun Nanofibers Measured *via* Polarized Raman Spectroscopy. *Nano Lett.* **2006**, *6*, 2526–2530.
37. Jaeger, R.; Schonherr, H.; Vancso, G. J. Chain Packing in Electro-spun Poly(ethylene oxide) Visualized by Atomic Force Microscopy. *Macromolecules* **1996**, *29*, 7634–7636.
38. Dersch, R.; Liu, T. Q.; Schaper, A. K.; Greiner, A.; Wendorff, J. H. Electrospun Nanofibers: Internal Structure and Intrinsic Orientation. *J. Polym. Sci., Part A* **2003**, *41*, 545–553.
39. Buzarovska, A.; Koseva, S.; Cvetkovska, M.; Nedkov, E. Poly(ethylene oxide) Blends with Poly(ethylene oxide)/Poly(dicyclohexyl itaconate) Block Copolymers. *Eur. Polym. J.* **2001**, *37*, 141–149.